FOLDING AND DEPLOYMENT OF ULTRA-THIN COMPOSITE STRUCTURES

H.M.Y.C. Mallikarachchi[(1)], **S. Pellegrino**[(2)]

[(1)]**University of Cambridge**
Department of Engineering, Trumpington Street, Cambridge CB2 1PZ, U.K.

[(2)]**California Institute of Technology**
1200 E. California Blvd., Pasadena, CA 91125
sergiop@caltech.edu

ABSTRACT

This paper presents an optimization study of thin-walled tape spring hinges made from carbon fiber reinforced plastic. Previously developed numerical simulation techniques to analyze the folding and deployment of these hinges are used to carry out a series of sensitivity studies. Starting from a reference hinge design, it is shown that the maximum mid-plane strain in the folded configuration can be reduced by a factor of 5 if an optimal length of the tape springs is chosen. An additional factor of 5 reduction can be achieved if prior to folding one compresses the whole hinge and so reduce its overall thickness to half.

1. INTRODUCTION

Stored energy deployable structures made of composite materials have several advantages over traditional deployable structures with mechanical joints. Their lightness, lower cost due to a smaller number of components, and behavior insensitive to friction are distinctive advantages. Structures based on this approach have already been used in a few missions and a range of novel structural architectures that exploit this approach in future missions has been proposed. For example, Astro Aerospace Flattenable Foldable Tubes (FFT) were used as deployable antennas on MARSIS [1], and RUAG's self-motorized deployment mechanism [2] and DLR's lightweight deployable booms [3] are examples of recent technology developments for future missions.

We are doing research on this kind of structures, with focus on a self-deployable hinge that is made by cutting longitudinal slots in a lightweight, thin-walled composite tube. We have already completed in-depth studies of the quasi-static and dynamic deployment behavior a particular hinge [4-6] made of two-ply ± 45 plain weave carbon fiber reinforced polymer (CFRP) material. The focus of the present paper is to use the simulation tools from our previous research to arrive at optimized designs for the geometry of the hinge. The material of the hinge is also being optimized, for example by varying the type of fabric, e.g. plain weave or tri-axial weave, the number of plies and the ply arrangement, but in this paper we will focus on the hinge geometry. We consider tubes with an internal diameter of 38 mm, thickness of 0.2 mm and areal density of 260 g/m^2.

During previous studies [6] it was observed that in the selected hinge geometry the highest strains in the deployed configuration occur near the transition between the straight and circular parts of the slots. In order to improve the hinge geometry we have chosen the basic configuration shown in Figure 1; the three parameters selected for the sensitivity analyzes are the slot length, L, the slot width, SW, and the diameter of the end circles, D.

We have explored the sensitivity of the hinge design to these three parameters by computing the maximum mid-surface strains in the fiber direction in the folded configuration for hinges with different geometries. This strain value provides a good measure of how close to failure a hinge gets when it is folded and deployed. As an alternative to this approach, we have computed the maximum mid-surface strains in folded configurations that are obtained through different folding processes. We have found that if we compress the whole hinge and so reduce its overall thickness to half prior to folding, and then fold by rotating the ends of the hinge as before, the maximum strains are reduced by a factor of 5.

2. NUMERICAL SIMULATIONS

We use the commercial finite element software ABAQUS/Explict for our simulations. Our model consists of

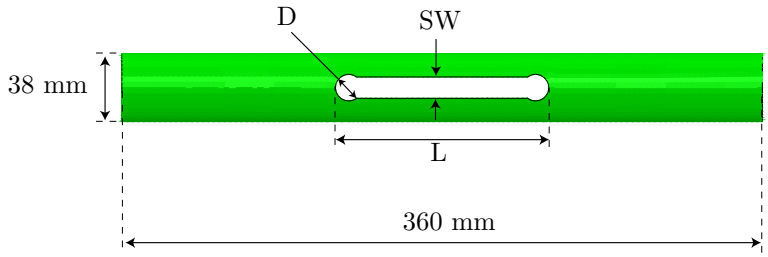

Figure 1: Hinge geometry.

a 360 mm long tube hinge held by two 25 mm wide Aluminum holders (which in the experiments reported in Ref. [4,6] were used to attach the hinge to a testing rig). The tube hinge is modeled with four node fully integrated shell elements, S4, with an approximate element size of 3 mm. The holders are modeled with four node reduced integrated shell elements, S4R with an approximate element length of 5 mm.

Each holder is attached to the tube hinge with surface based **Tie* constraints. This allows us to control the motion of the hinge by specifying boundary conditions on the two holders, Figure 2.

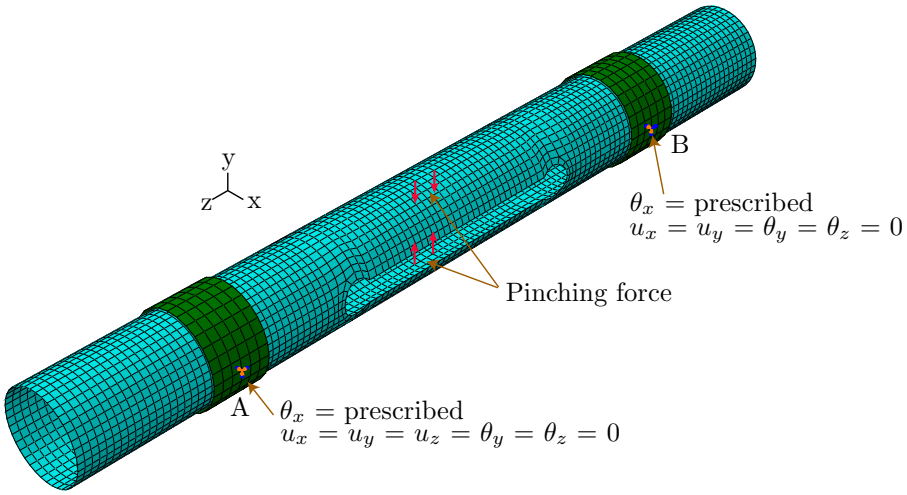

Figure 2: Finite element model.

The material properties are obtained through a separate micro-mechanical model which uses the concept of homogenization [6]. The ABD matrix computed using this approach is defined in ABAQUS using the command **Shell General Section*.

During this simulation different parts of the tube hinge come into contact with each other. This behavior is modeled by the **General contact* feature available in ABAQUS/Explicit.

A folding simulation is carried out in two stages. Because the hinge has a high bending stiffness in the fully deployed configuration, to reproduce the process of folding an actual hinge we begin by pinching the hinge in the middle by applying equal and opposite concentrated forces, as shown in Figure 2. Then the hinge is rotated by 170 deg by applying equal and opposite rotations on nodes A and B. To minimize the accelerations anywhere in the model, the end rotations are defined as a smooth fifth-order polynomial function of time (*Smooth Step* in ABAQUS). Also a viscous pressure load is applied over the complete hinge throughout the entire folding simulation to damp out any stress waves coming out of the tube surface [6,7]. A detailed description of the simulation technique is provided in our previous papers [4,6].

Figure 3 shows the energy variation corresponding to a folding simulation of a tube hinge with design parameters $SW = 10$ mm, $D = 15$ mm and $L = 120$ mm. Note that the kinetic energy is negligible compared to the internal energy which indicates that the response is quasi-static. Also the energy balance term is zero throughout the simulation which confirms that the simulation is free of numerical instabilities [6,8].

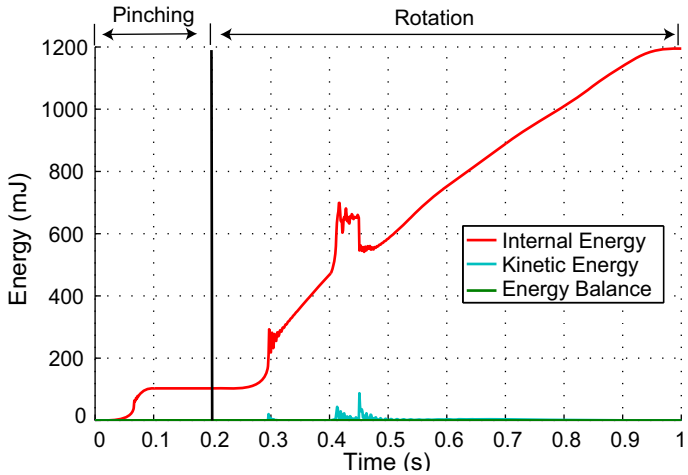

Figure 3: Energy variation ($SW = 10$ mm, $D = 15$ mm, $L = 120$ mm).

Key results from this simulation are presented in Figure 4 which shows the mid-surface strain and curvature distribution along the +45 deg fibers in the fully folded configuration. Note that the hinge is subjected to high mid-surface strains around the end of the slot, with a maximum of around 2.4%. The ultimate tensile strain of T300 fibers is only 1.5% [9] and hence this hinge could not be folded safely.

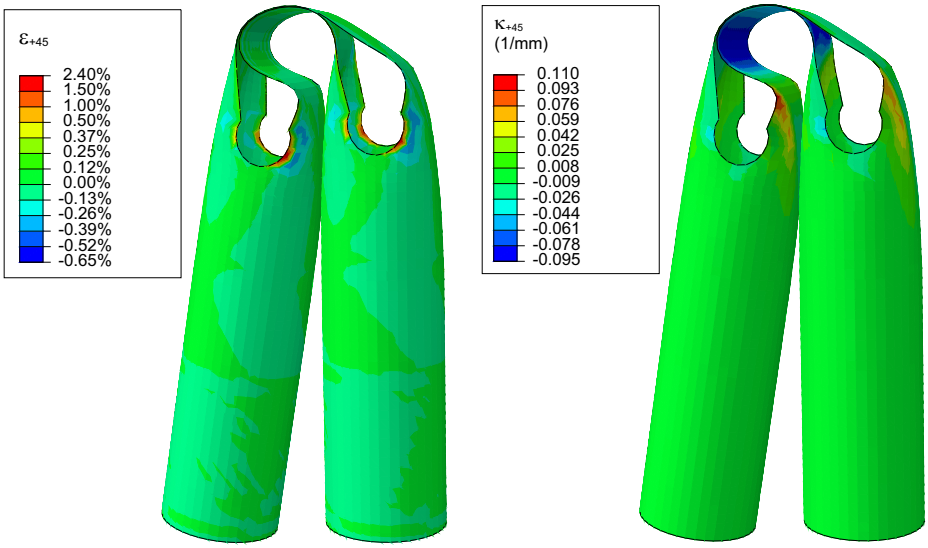

(a) Mid-plane strain (b) Mid-surface curvature

Figure 4: Mid-surface strain and curvature variation along +45 deg fibers in fully folded configuration (SW=10 mm, D=15 mm, L=120 mm).

3. IMPROVED GEOMETRIES

The sensitivity of the maximum mid-surface strain and the maximum curvature in the folded configuration has been studied.

3.1 Initial Studies

Initially we decided to vary the parameter L while keeping SW and D constant. L was varied from 60 mm to 140 mm while keeping $SW = 10$ mm and $D = 15$ mm. An additional case, with $SW = 15$ mm, $D = 20$ mm and $L = 120$ mm was also studied. Table 1 shows the maximum mid-surface strain in the +45 deg direction (parallel to one of the fiber directions), ε_{+45}, in the fully folded configuration for each case.

Table 1: Initial sensitivity analysis: maximum mid-surface strain in +45 deg direction in fully folded configuration.

Case No.	SW (mm)	L (mm)	D (mm)	ε_{+45} (%)
I	10	60	15	2.9
II	10	90	15	4.9
III	10	100	15	3.8
IV	10	120	15	2.4
V	10	140	15	0.3
VI	15	120	20	0.2

Note that apart from design no. V and VI the hinge is subjected to high mid-surface strains. In general, the maximum strain value decreases when the slot length is increased. The reason why design no. I has lower strain than design no. II is because in case I the tape strings are not long enough to form a 170 deg fold and hence they force the two end tubes against each other, Figure 5.

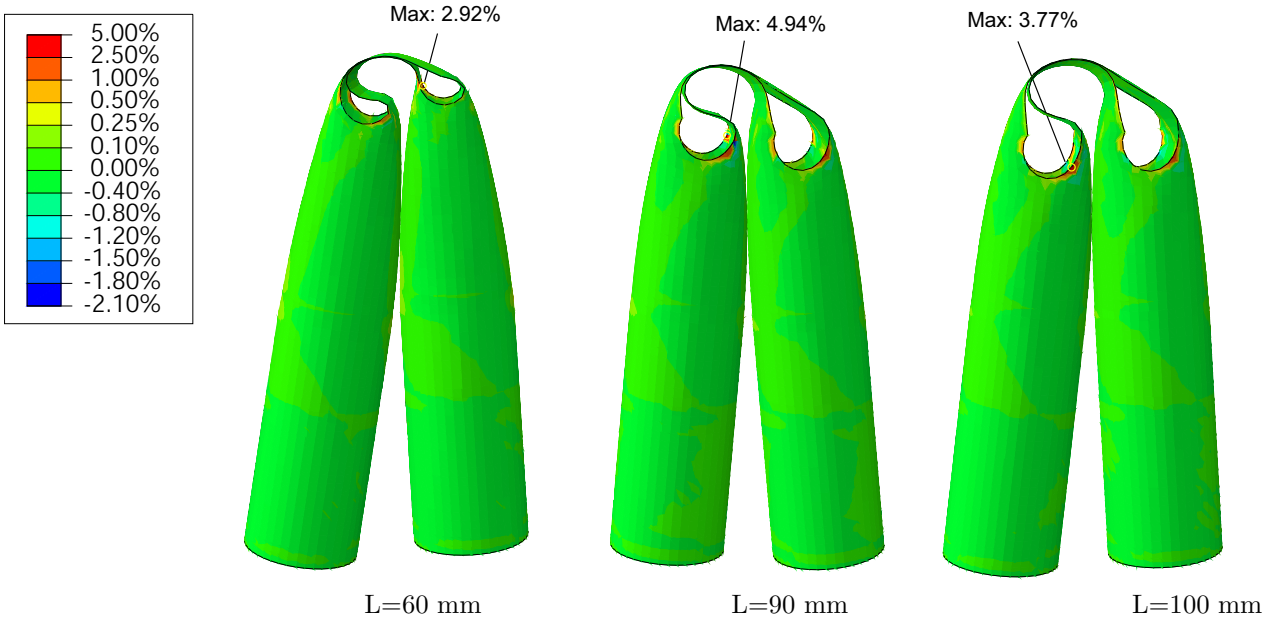

Figure 5: Mid-plane strain distribution along +45 deg fibers in cases I, II, III.

Note that case IV and VI have the same value of L but changes in SW and D bring down the maximum ε_{+45} by an order of magnitude.

3.2 Sensitivity to Slot Width

Next, the sensitivity to SW was studied. This was done by varying SW from 10 mm to 15 mm while keeping $D = 15$ mm and $L = 120$ mm, Table 2. Figures 6a and 6b show the variation of the maximum mid-surface strains and curvatures along +45 deg fibers, respectively. Note that the strains show a significant sensitivity to SW but the curvatures are fairly insensitive.

SW (mm)	ε_{+45} (%)	ε_{-45} (%)	$\varepsilon_{\pm 45}$ (%)	κ_{+45} (1/mm)	κ_{-45} (1/mm)	$\kappa_{\pm 45}$ (1/mm)
10	2.40	2.21	1.86	0.110	0.112	0.126
11	1.91	1.60	1.63	0.111	0.112	0.132
12	1.81	1.79	1.49	0.111	0.109	0.133
13	0.23	0.21	0.79	0.087	0.087	0.131
14	0.22	0.20	0.75	0.087	0.087	0.132
15	1.88	1.73	1.23	0.108	0.108	0.141

Table 2: Mid-plane strain and curvature components along +45 deg fibers with varying SW ($D = 15$ mm, $L = 120$ mm).

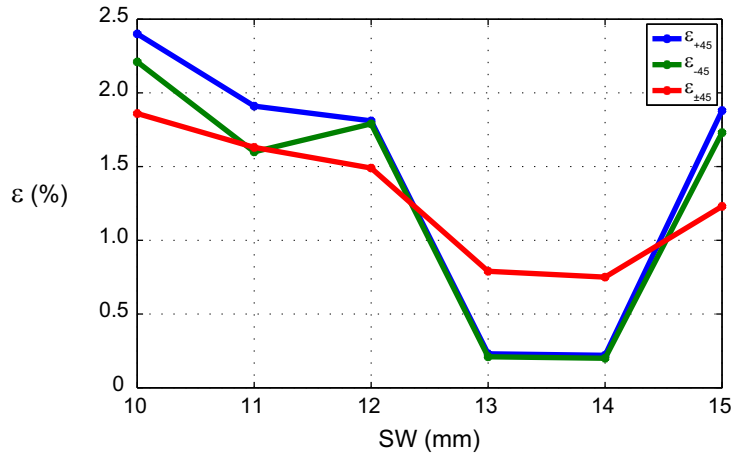

(a) Strain

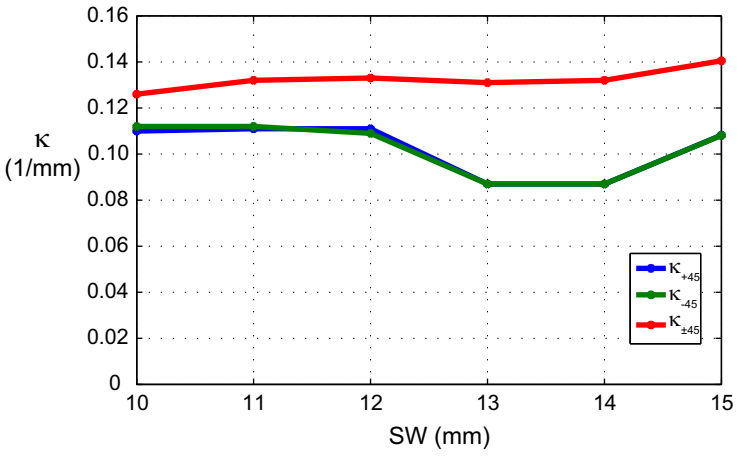

(b) Curvature

Figure 6: Variation of maximum mid-surface strains and curvatures with SW.

3.3 Sensitivity to Slot Length

According to Section 3.2, choosing SW in the range 13 mm to 14 mm reduces the mid-surface strains by an order of magnitude. Hence $SW = 13$ mm and $D = 15$ mm were selected as constants and L was varied from 120 mm to 110 mm in 2 mm increments. Table 3 shows the maximum mid-surface strains and curvature components along +45 deg fibers.

L (mm)	ε_{+45} (%)	ε_{-45} (%)	$\varepsilon_{\pm 45}$ (%)	κ_{+45} (1/mm)	κ_{-45} (1/mm)	$\kappa_{\pm 45}$ (1/mm)
120	0.23	0.21	0.79	0.087	0.087	0.131
118	1.92	1.70	1.57	0.116	0.115	0.137
116	1.99	1.73	1.58	0.120	0.120	0.136
114	0.25	0.25	0.83	0.090	0.089	0.135
112	2.43	2.24	1.84	0.123	0.126	0.141
110	2.15	1.88	1.66	0.118	0.120	0.148

Table 3: Mid-surface strain and curvature components along +45 deg fibers with varying L ($SW = 13$ mm, $D = 15$ mm).

The maximum strains for the cases $L = 114$ mm and $L = 120$ mm are significantly lower than the rest; in all other cases the maximum strain is higher than the ultimate tensile strain of T300 fibers, Figure 7a. Also, similarly to the sensitivity to SW the curvatures do not show a significant variation, Figure 7b.

4. SENSITIVITY TO MESH REFINEMENT

In Section 3 we have considered only the maximum strain and curvature values. Hence it is important to establish how sensitive these peak values might be to the mesh refinement.

We selected as test case with high mid-surface strains the design with $SW = 13$ mm, $D = 15$ mm and $L = 118$ mm and this particular hinge was meshed with three different element sizes as shown below.

- Mesh 1 : approximate element length of 3 mm, Figure 8a.
- Mesh 2 : approximate element length of 2 mm, Figure 8b.
- Mesh 3 : approximate element length of 2 mm, refined mesh around the end circles of the slot, Figure 8c.

Figure 9(a) and (b) shows the distribution of mid-surface strains along +45 deg fibers in the fully folded configuration, for Mesh 1 and Mesh 2, respectively. Note that high strains occur around the circular ends of the slot while everywhere else they are approximately the same. Table 4 shows the variation of the maximum mid-surface strains and curvatures with the mesh refinement. Note that the values of the maximum normal strains drop by around 30%, the maximum shear strain increases, and the curvatures remain approximately unchanged. This variability is much smaller than that established in Section 3 and so the sensitivity of the maximum mid-surface strains to SW and L has been confirmed.

Mesh	ε_{+45} (%)	ε_{-45} (%)	$\varepsilon_{\pm 45}$ (%)	κ_{+45} (1/mm)	κ_{-45} (1/mm)	$\kappa_{\pm 45}$ (1/mm)
Mesh 1	1.92	1.70	1.57	0.116	0.115	0.137
Mesh 2	1.35	1.37	1.72	0.119	0.119	0.154
Mesh 3	1.20	1.31	1.68	0.119	0.119	0.155

Table 4: Sensitivity to mesh refinement ($SW = 13$ mm, $D = 15$ mm and $L = 118$ mm)

5. ALTERNATIVE FOLDING SEQUENCE

The initial sensitivity study in Section 3 has shown that the maximum mid-surface strains are reduced when

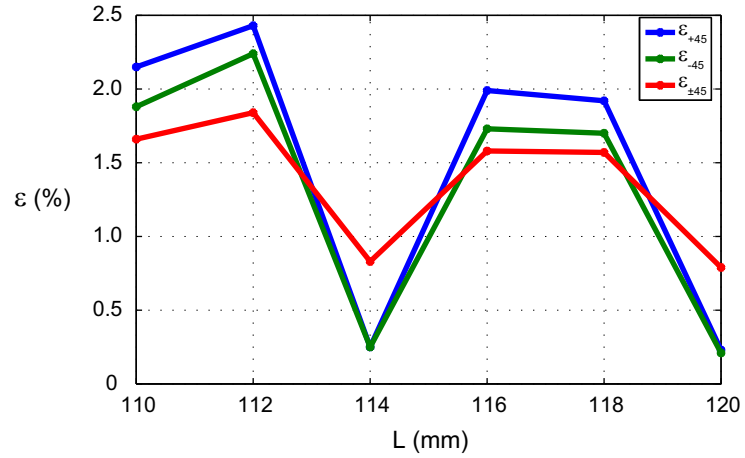

(a) Strain

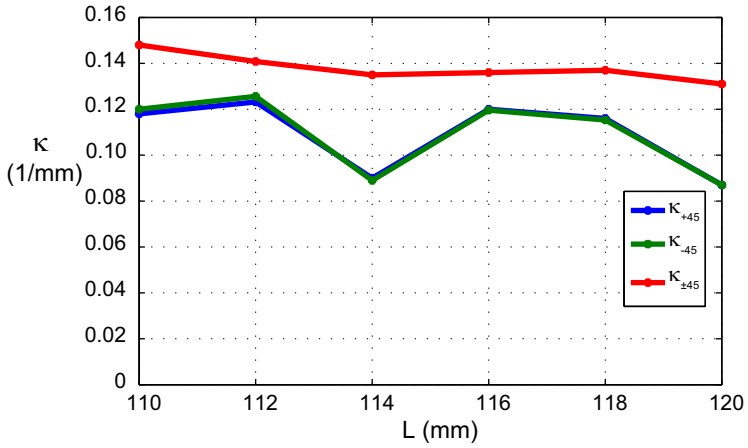

(b) Curvature

Figure 7: Variation of mid-surface strains and curvatures with L ($SW = 13$ mm, $D = 15$ mm)

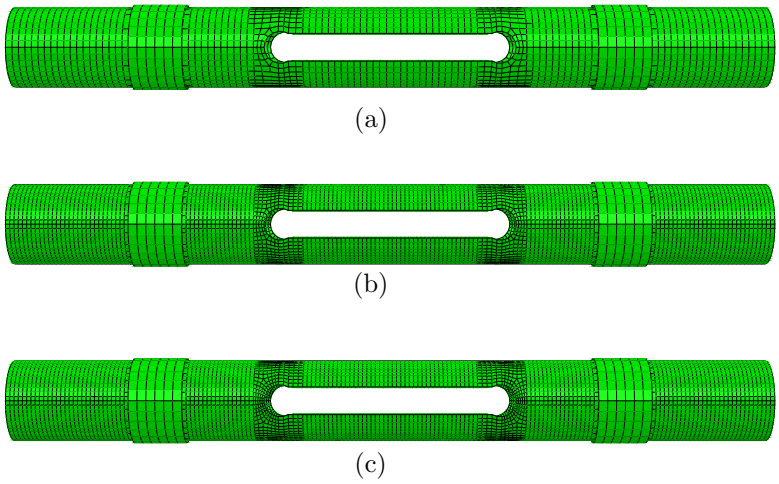

(a)

(b)

(c)

Figure 8: Mesh refinement study ($SW = 13$ mm, $D = 15$ mm and $L = 118$ mm).

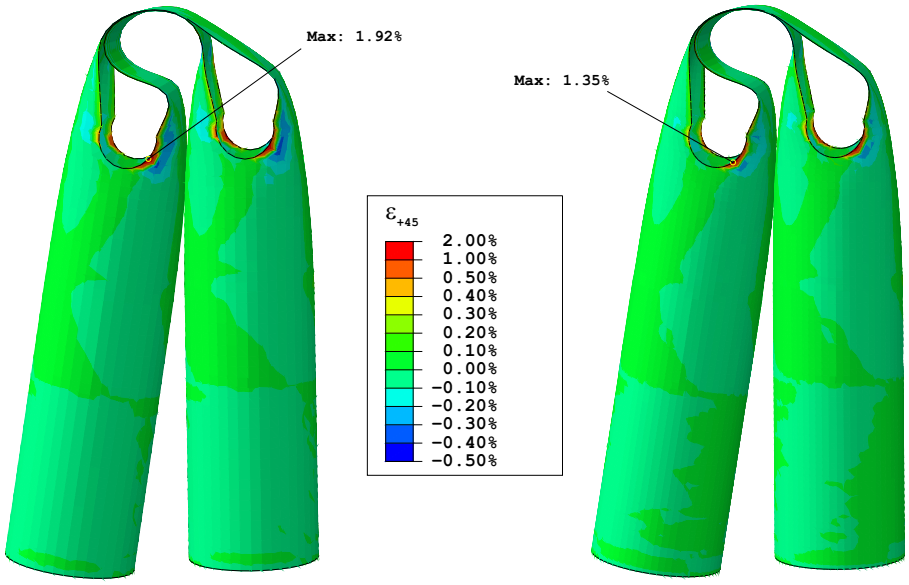

(a) (b)

Figure 9: Sensitivity to mesh refinement ($SW = 13$ mm, $D = 15$ mm and $L = 118$ mm)

the hinge is compressed. This observation prompted us to start investigating the effect of the folding process on the maximum strains in the folded configuration.

In the finite element model presented in Section 2 the Aluminium holders prevent the distortion of the cross-sections of the tube near the ends and hence prevent overall flattening of the hinge. Since this distortion may be beneficial in reducing the strains, a new model has been created by removing the two Aluminium holders.

The alternative folding sequence consists in first flattening the hinge to half of its cross-sectional diameter while pinching it in the middle and then folding by rotating the two ends, Figure 10.

Figure 11 shows the mid-surface strain variation in the +45 deg fibers for a hinge with $SW = 10$ mm, $D = 15$ mm and $L = 60$ mm. Note that the maximum strain has decreased from 2.92% to 0.52% with the new folding technique.

6. DISCUSSION

In the case studies presented in this paper only the mid-surface strain and curvature components in the fiber directions, were analyzed. Ideally we should compute the maximum surface strain by applying all deformation components at the same time to the homogenized unit cell model and then compare them with the ultimate strains of the fibers and the matrix [6].

We are currently working on refining these results and we plan to extend this work to dynamic deployment. Also some optimized hinges will be constructed and tested and hence the results of the present optimization study will be experimentally validated.

REFERENCES

[1] Adams, D.S. and Mobrem, M. "Lenticular Jointed Antenna Deployment Anomaly and Resolution Onboard the Mars Express Spacecraft", *Journal of Spacecraft and Rockets*, Vol. 46, No. 2, pp. 403–410, 2009.

[2] Boesch, C., Pereira, C., John, R., Schmidt, T., Seifart, K., Sparr, H., Lautier, J.M., Pyttel, T. "Ultra Light Self-Motorized Mechanism for Deployment of Light Weight Space Craft Appendages", *39th Proceedings of Aerospace Mechanisms Symposium*, 7-9 May 2008, Newport, NASA Marshall Space Flight Center, 2008.

[3] Sickinger, C., Herbeck, L., Strohelin, T., Torrez-Torres, J. "Lightweight Deployable Booms: Design, Manufacture, Verification, and Smart Materials Application", *55th International Astronautical Congress*

of IAF/IAA/IISL, October 04 - 08 2004, Vancouver, Canada.

[4] Mallikarachchi, H.M.Y.C. and Pellegrino, S. "Simulation of Quasi-Static Folding and Deployment of Ultra-Thin Composite Structures", *49th AIAA/ASME/ASCE/AHS/ASC Structures, Structural Dynamics, and Materials Conference*, AIAA-2008-2053, Schaumburg, Illinois, 07-10 April 2008.

[5] Mallikarachchi, H.M.Y.C. and Pellegrino, S. "Deployment Dynamics of Composite Booms with Integral Slotted Hinges", *50th AIAA/ASME/ASCE/AHS/ASC Structures, Structural Dynamics, and Materials Conference*, AIAA-2009-2631, Palm Springs, California, 4 - 7 May.

[6] Mallikarachchi, H.M.Y.C. and Pellegrino, S. "Quasi- Static Folding and Deployment of Ultra-Thin Composite Structures", submitted for publication.

[7] SIMULIA, ABAQUS/Explicit Version 6.7, Providence, RI.

[8] Belytschko, T., Liu, W.K. and Moran, B. "6.2.3 Energy balance", *Nonlinear Finite Elements for Continua and Structures,* Chichester, J. Wiley & Sons, pp. 315-316, 2000.

[9] Torayca. Technical Data Sheet No. CFA-001, T300 Data Sheet.

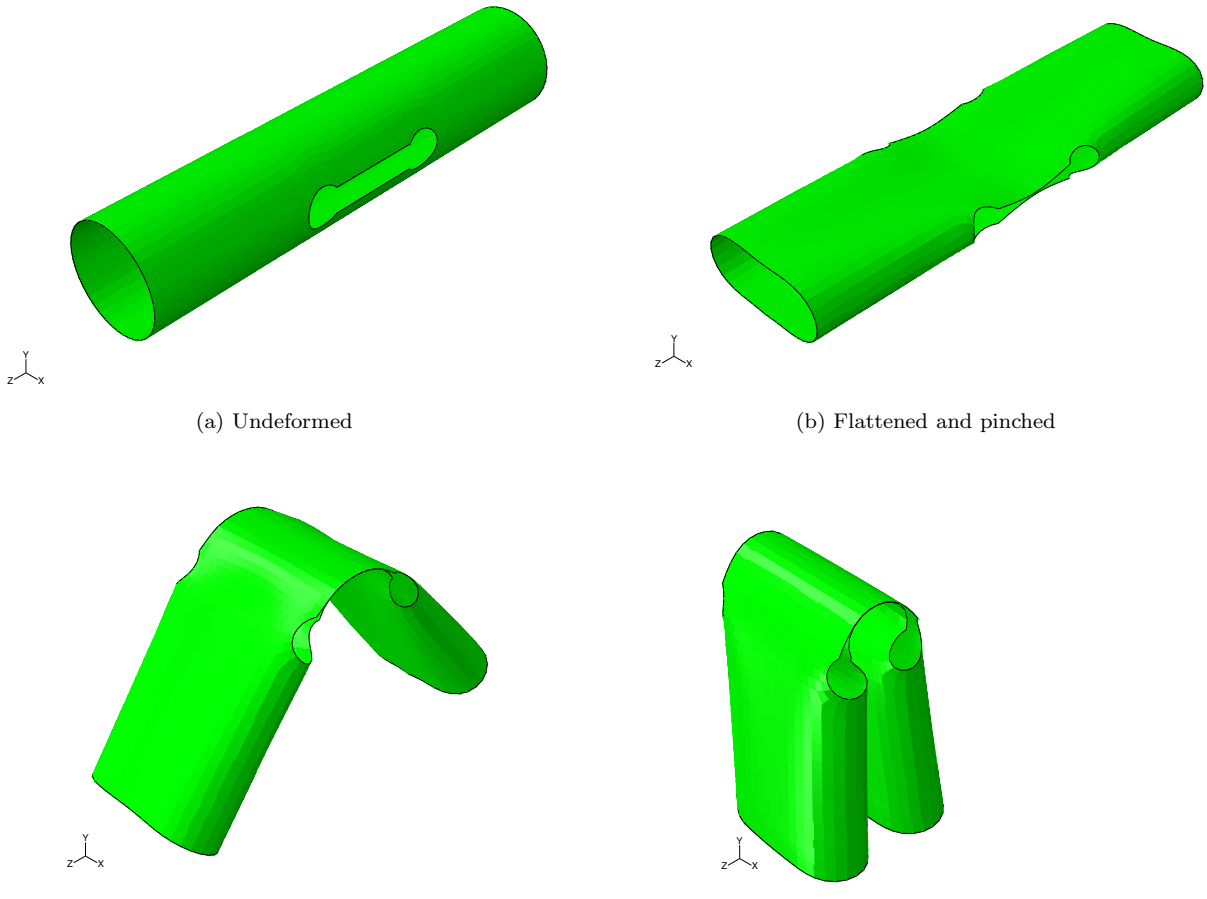

(a) Undeformed

(b) Flattened and pinched

(c) Rotating

(d) Fully folded

Figure 10: Alternative folding sequence.

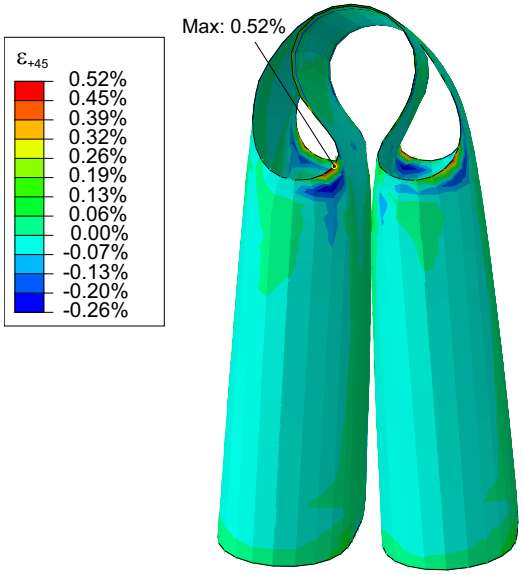

Figure 11: Mid-surface strains along +45 deg fibers for $SW = 10$ mm, $L = 60$ mm, $D = 15$ mm.